



**HAL**  
open science

## Functionalized 2D nanolaminate membranes for nanofluidics and molecular sieving

Wensen Wang, Xinsheng Peng, Chrystelle Salameh, Zhiyuan Zeng, Damien Voiry

► **To cite this version:**

Wensen Wang, Xinsheng Peng, Chrystelle Salameh, Zhiyuan Zeng, Damien Voiry. Functionalized 2D nanolaminate membranes for nanofluidics and molecular sieving. Trends in Chemistry, 2024, 6 (6), pp.285-301. 10.1016/j.trechm.2024.04.006 . hal-04747975

**HAL Id: hal-04747975**

**<https://hal.science/hal-04747975v1>**

Submitted on 22 Oct 2024

**HAL** is a multi-disciplinary open access archive for the deposit and dissemination of scientific research documents, whether they are published or not. The documents may come from teaching and research institutions in France or abroad, or from public or private research centers.

L'archive ouverte pluridisciplinaire **HAL**, est destinée au dépôt et à la diffusion de documents scientifiques de niveau recherche, publiés ou non, émanant des établissements d'enseignement et de recherche français ou étrangers, des laboratoires publics ou privés.

# Functionalized Two-Dimensional Nanolaminate Membranes For Nanofluidics And Molecular Sieving

Wensen Wang<sup>1</sup>, Xinsheng Peng<sup>2,3</sup>, Chrystelle Salameh<sup>1</sup>, Zhiyuan Zeng,<sup>4,5</sup> Damien Voiry<sup>1\*</sup>

<sup>1</sup> *Institut Européen des Membranes, IEM, UMR 5635, Université Montpellier, ENSCM, CNRS, Montpellier 34000, France*

<sup>2</sup> *State Key Laboratory of Silicon Materials, School of Materials Science and Engineering, Zhejiang University, Hangzhou 310027, P. R. China*

<sup>3</sup> *Wenzhou Key Laboratory of Novel Optoelectronic and Nanomaterials, Institute of Wenzhou, Zhejiang University, Wenzhou 325006, P. R. China*

<sup>4</sup> *Department of Materials Science and Engineering, City University of Hong Kong, Hong Kong 999077, P. R. China*

<sup>5</sup> *Shenzhen Research Institute, City University of Hong Kong, Shenzhen 518057, China*

## Abstract

Two-dimensional (2D) material nanolaminate membranes (2DMMs) have garnered significant attention as next-generation separation membranes thanks to their superior molecular permeation properties and remarkable selectivity. The performance of 2DMMs is largely determined by nanochannel architecture and microenvironment, which are affected by the surface pattern and physicochemical properties of 2D nanosheets.

This review summarizes the nanochemistry strategies for engineering 2D materials and discusses the effect of nanosheet modification on the nanochannel architecture (interlayer space) and surface physicochemical properties (charge, affinity, and hydrophilicity) of the nanolaminate membrane. It also sheds light on the importance of the physical and chemical properties of the nanosheets in tailoring the performance of 2DMMs for selective sieving. We finally discuss the remaining challenges and

29 opportunities associated with the development of 2DMMs.

30

### 31 **2D materials as separation membranes**

32 Membrane separation is an energy-efficient and environmentally friendly method  
33 that has found widespread use in gas separation, ionic sieving, water purification, and  
34 seawater desalination [1,2]. **Membranes** (see Glossary) play a crucial role in the  
35 performance of separation techniques, and as such, there is an ongoing pursuit for better  
36 membranes with higher permeability, greater **rejection**, and improved stability.

37 Polymer membranes have dominated the separation membranes market due to their  
38 abundant species, easy processing, and scalability. However, the performance of  
39 conventional polymer membranes has hit an upper limit due to the trade-off between  
40 permeability and rejection [3]. Moreover, plasticization and fouling of polymer  
41 membranes can significantly degrade their performance and shorten their service life  
42 [4]. The search for new materials with high permeability and rejection as next-  
43 generation separation membranes has become a research hotspot.

44 **Two-dimensional (2D) materials** possess unique advantage in membrane separation  
45 due to their atomic thickness and large-lateral surfaces with abundant active sites and  
46 tunable charge density to construct channels with confined environments and have been  
47 proposed as membrane building blocks [5,6].

48 2D single-layer membranes consist of a single or a few-layer perforated nanosheets  
49 supported by a porous substrate (Figure 1A). The selectivity is achieved by the different  
50 permeation rates through the nanopores on the nanosheets, which are caused by size  
51 confinement, electrostatic interaction, and chemical or physical adsorption [9].

52 Conversely, 2D nanolaminate membranes are assembled by stacking 2D nanosheets,  
53 and the mass transport occurs in the confined interlayer **nanochannels** formed between

54 two adjacent nanosheets (Figure 1B) as well as in the intraplanar channels formed by  
55 intrinsic or perforated nanopores on nanosheets. High selectivity is typically achieved  
56 through sized exclusion, electrostatic repulsion, or adsorption inside the nanochannels  
57 [6]. By optimizing the interstitial nanostructure together with the physical and chemical  
58 properties of the nanosheet surface, nanolaminate membranes hold potential for  
59 breaking the permeability and selectivity tradeoff in traditional membranes.

60 Up to now, several important milestones have been achieved both in single-layer  
61 membranes and nanolaminate membranes. Different types of 2D materials with  
62 intrinsic nanoporosity such as metal-organic frameworks (MOFs), covalent organic  
63 frameworks (COFs) and zeolite have been demonstrated [7,8]. These membrane  
64 building blocks have precise pore sizes ranging from subnanometer to tens of  
65 nanometers, offering promising prospects for fast ionic sieving and molecular  
66 separation [10-13]. Various perforation methods such as ion/electron beam irradiation,  
67 oxygen plasma etching, and ultraviolet-induced etching have been successfully used to  
68 create pores on nonporous nanosheets like porous graphene and MoS<sub>2</sub>, resulting in  
69 single-layer membranes with ultrahigh permeability approaching the theoretical limit  
70 [14-16]. Despite the significant progress, single- and few-layer membranes still face  
71 two main challenges; namely (1) the synthesis of integrated large-scale nanosheets  
72 without defects/voids remains a challenge and (2) the poor mechanical strength  
73 resulting from their atomic thickness and high-density pore distribution on the  
74 nanosheets limits their practical applications. Comparatively, nanolaminate membranes  
75 significantly reduce the probability of pinholes and increase mechanical strength,  
76 making them more suitable for real separation processes and higher-pressure operations.

77 For nanolaminate membranes, the transport and sieving phenomena primarily occur  
78 in the interlayer nanochannels, which are regulated by their nanostructure and surface

79 physicochemical properties. Nanochemistry approaches have been proposed to  
80 engineer exfoliated nanosheets by attaching various groups, molecules, ions, or  
81 nanoparticles to their surfaces. These modifications are typically achieved through  
82 covalent or non-covalent strategies (*Boxes 1*, Figure I). Although nanolaminate  
83 membranes have been previously discussed in the literature [17,18], most of them are  
84 material-oriented reviews, focusing only on one typical membrane, such as GO, MoS<sub>2</sub>  
85 or MXene-based membranes. The present review aims to go beyond by exposing the  
86 recent developments in the engineering of the surface chemistry and the interlayer of  
87 2D nanolaminates. This review will provide an original in-depth discussion on the two  
88 important research area associated with nanolaminate membranes: (1) the chemical  
89 modifications of exfoliated nanosheets and (2) the consequences on the nanostructure  
90 and microenvironment of membranes. By using selected examples from the literature,  
91 we will examine how surface engineering of the nanosheets can tailor the nanochannel  
92 architecture (**interlayer space**), the surface physicochemical properties (charge,  
93 affinity, and hydrophilicity), and the resulting separation properties. We finally provide  
94 an outlook on the remaining challenges and opportunities for 2D nanolaminate  
95 membranes towards realistic applications.

96

97 ***Box 1. Nanosheets modification strategies employed in nanolaminate***  
98 ***membranes***

99 *Thanks to their large specific surface area, surface modification of the exfoliated 2D*  
100 *nanosheets via covalent or non-covalent strategies has proven to be an efficient*  
101 *strategy to tailor the local microenvironment of the nanolaminates (Figure I). Covalent*  
102 ***functionalization*** *allows the stable attachment of molecules to the edges or the basal*  
103 *planes of exfoliated nanosheets. Due to the absence of dangling bonds on the basal*

104 *planes of pristine 2D materials, covalent functionalization often necessitates the use of*  
105 *highly reactive reagents. This includes strong oxidants, reducing agents, nucleophiles,*  
106 *electrophiles, among others depending on the targeted reaction and the nature of the*  
107 *2D material. Remarkably, functionalized nanosheets can be modified further by*  
108 *attaching more complex molecules using substitution, amidation, silanization and*  
109 *esterification reactions with the heteroatoms on their surfaces, such as -F, -OH, and -*  
110 *COOH groups [29,30]. Non-covalent functionalization of nanosheets has emerged as*  
111 *a promising approach to modify exfoliated nanosheets without inducing defects. This*  
112 *strategy takes advantage of attractive interactions, such as electrostatic and van der*  
113 *Waals forces or hydrogen bonding, rather than covalent bonding. The ions, molecules*  
114 *and polymers are commonly employed to attach to the 2D nanosheets surface. Non-*  
115 *covalent functionalization can also involve the use of nanospacers that physically*  
116 *interact with the surface of nanosheets. These spacers consist of 1D or 0D nanoobjects,*  
117 *which are typically mixed together with the 2D nanosheets before the nanolaminate*  
118 *assembly, and the resulting membranes can be viewed as composite structures.*  
119 *In the context of engineering nanolaminate membranes, both functionalization*  
120 *strategies offer complementary advantages. For instance, compared to covalent*  
121 *functionalization, non-covalent functionalization is simpler to implement and more*  
122 *versatile in terms of available functionalization strategies and the types of molecules,*  
123 *ions, or nanospacers that can be used. Covalent functionalization of 2D materials*  
124 *typically involves the formation of defects that act as anchor sites, potentially altering*  
125 *the structure of the nanosheets over time. However, covalent bonding provides*  
126 *robustness and stability, preventing the leaching of intercalants during operation and*  
127 *thereby limiting contamination of the permeate solution.*

128

## Engineering of the interlayer space

The interlayer space between adjacent nanosheets is crucial for solvent transport and molecular sieving in nanolaminate membranes. As the diffusion of chemical species mainly occurs in the interlayer nanochannel, the functional groups grafted onto nanosheets act as pillars to increase the interlayer space. The role of the interlayer space in nanolaminate membranes can be perfectly illustrated by the example of graphene (Box 2). MoS<sub>2</sub>, one of the most extensively studied TMDs, encounters similar challenges as graphene. In dry conditions, Wang *et al.* found that MoS<sub>2</sub> laminate membranes exhibit a d-space of around 0.62 nm, corresponding in a **capillary width** of less than 0.15 Å [61]. While the strong van der Waals forces can maintain this d-space in water, it renders the membrane impermeable to water molecules. The covalently functionalized MoS<sub>2</sub> membranes show an expanded interlayer space (Figure 2B) [62]. The meticulous selection of functional groups enables precise control of the interlayer spacing from 9.8 Å to 13.3 Å, tuned with ångström precision [63]. This modification provides high water permeability and highly efficient desalination performance [62-64]. Additional studies by Hoenig *et al.* have confirmed that this functionalization strategy effectively facilitates water transport pathways in MoS<sub>2</sub> nanolaminates [65].

### ***Box 2. Water diffusion in graphene and graphene oxide nanolaminates***

*In hydrophobic graphene and carbon nanotubes, water molecules can diffuse by slipping at the liquid/solid interface. The **slip length**, which is defined as the extrapolated distance relative to the wall where the tangential velocity component vanishes, can reach several hundred nanometers inside carbon nanotubes and tens of nanometers in graphene capillaries [54,55]. This large slip length in graphene and*

154 carbon nanotubes is of quantum origin, as recently identified [56]. Multilayer graphene  
155 membranes possess laminate structures with turbo-stacked nanosheets creating an  
156 interlayer space of  $\sim 0.34$  nm. However, this size is insufficient to allow for the transport  
157 of small molecules (Figure 2A). Graphene oxide (GO), the oxidized counterpart of  
158 graphene, is one of the most studied 2D materials due to its ease of preparation and  
159 high stability in solution when exfoliated. GO nanolaminates, with an interlayer  
160 distance of 0.8 nm created by the oxygenated groups acting as pillars, are suitable for  
161 small molecule transport, such as  $H_2$  [57]. In graphene oxide, the functional groups  
162 allow chemical species to diffuse by increasing the interlayer distance, while the  
163 pristine conjugated and hydrophobic regions of graphene allow a fast diffusion of water  
164 molecules. The oxygen-containing groups of GO however turn graphene nanosheets  
165 hydrophilic, leading to a larger friction force between water molecules and the  
166 capillary walls and a reduced rate of water diffusion [58]. By contrast, hydrophobic  
167 surfaces minimize friction during water diffusion, leading to faster flow. The slip length  
168 of water in graphene oxide decreases to 1-2 nm due to the presence of functional groups  
169 on the nanosheets and the subsequent modification of the surface properties. This  
170 behavior has been confirmed experimentally and investigated by several theoretical  
171 studies, which have highlighted the unique properties of graphene oxide nanosheets as  
172 membrane building blocks [59,60].

173

174 In MXene nanolaminate membranes, the presence of terminated -F and -OH groups  
175 results in extremely small capillary widths. This unique characteristic contributes to  
176 high hydrogen ( $H_2$ ) permeation rates compared to other common gas molecules like  
177  $CO_2$ ,  $N_2$ , and  $CH_4$  [66]. To increase the interlayer space of MXene nanolaminate  
178 membranes for solvent transport, silane coupling agents have successfully been



179 employed to react with surface -OH groups. By utilizing silane-functionalized MXene,  
180 the interlayer space is effectively increased, thereby enabling enhanced solvent  
181 permeability through the membranes [67].

182 Functional groups play a crucial role in opening up the interlayer space of  
183 nanosheets. However, when hydrophilic groups, such as oxygenated groups, are grafted  
184 onto the nanosheet surface, a potential issue arises when operating the membranes in  
185 aqueous solutions. This is due to the propensity of these hydrophilic groups to cause  
186 swelling, which can lead to an undesired increase in interlayer spacing. Additionally,  
187 as penetrants diffuse within the tortuous transmembrane pathway, they can reduce the  
188 interactions between the nanosheets, ultimately resulting in the delamination of the  
189 membrane structure. These factors combined can contribute to an increased interlayer  
190 space, ultimately leading to poorer sieving performance in the membranes. In this  
191 context, an effective strategy for tackling the challenges linked to swelling and  
192 uncontrolled fluctuations in the interlayer spacing of nanolaminate membranes is to  
193 incorporate bridging molecules capable of crosslinking adjacent nanosheets. These  
194 bridging molecules react with the existing functional groups on the nanosheet surface,  
195 effectively fixing the interlayer space and limiting undesired swelling. By introducing  
196 crosslinking agents, the nanosheet structure is reinforced, enhancing the stability and  
197 preventing excessive expansion of the interlayer space. Hung *et al.* employed diamines  
198 with different sizes to crosslink GO nanosheets and tune the interlayer space, while  
199 demonstrating a limited swelling in water (Figure 2C) [68]. The crosslinked GO  
200 membranes show highly efficient and long-time stable ethanol dehydration  
201 performance under pervaporation. A similar strategy has been widely applied to GO  
202 laminate membranes for the different separation applications, such as ionic sieving [69],  
203 water purification and desalination [70] and organic solvent nanofiltration [71]. In

204 addition to diamine, other compounds such as organic acids (dicarboxylic acids) [72]  
205 and inorganic acids (boric acid) [73] have been successfully used for crosslinking GO  
206 (graphene oxide) nanosheets to address interlayer spacing issues. Thiourea, urea, diols  
207 and dopamine with available -NH<sub>2</sub> and -OH groups in the end are also employed to  
208 react with the oxidation groups on GO nanosheets to stabilize the nanochannels in  
209 nanolaminate membrane [74].

210

211 Non-covalent strategies allow for easy and reversible modifications, making it  
212 particularly attractive for fine-tuning the behavior of nanosheets in nanochannels.  
213 Intercalated ions within the nanochannels serve a dual role: enhancing the stability and  
214 mechanical strength of membranes through strong electrostatic attractions and  
215 mitigating swelling effects. Chen *et al.* firstly use different cations (K<sup>+</sup>, Na<sup>+</sup>, Ca<sup>2+</sup>, Li<sup>+</sup>  
216 and Mg<sup>2+</sup>) to decorate the GO nanolaminate membrane, showcasing the ability to finely  
217 tune the interlayer spacing with remarkable precision, ranging from 11.4 Å to 13.6 Å  
218 in aqueous solutions [31]. The strong cation- $\pi$  interactions between hydrated cations  
219 and the aromatic rings from GO nanosheets and electrostatic attraction are responsible  
220 for the contracted interlayer space, which can efficiently and selectively exclude other  
221 ions that have larger hydrated volumes, demonstrating great promise for precise ion and  
222 molecular sieving in aqueous solutions. The ion modification strategy has also proven  
223 successful in negatively charged MXene membranes. Multivalent ions and poly-cations  
224 have been tested for controlling the swelling of MXene membranes, [75] [38] [33]. By  
225 introducing Al<sup>3+</sup> or Ca<sup>2+</sup> ions into the interlayer spaces, the swelling of MXene  
226 membranes can be effectively limited and regulated [38] [33]. Similar to GO  
227 nanolaminates, the controlled swelling ensures a fixed interlayer spacing, which in turn  
228 contributes to highly efficient desalination performance in both forward and reverse

229 osmosis processes.

230 Nanoparticles and polymers, characterized by their larger size compared to ions  
231 and molecules, have been investigated as spacers. The utilization of SiO<sub>2</sub> nanoparticles  
232 to decorate GO nanosheets, for instance, results in the formation of an hourglass-shaped  
233 nanochannel structure that is analogous to the conformation of water transport proteins  
234 in GO nanolaminate membranes [52]. The resulting heterostructure design provides a  
235 wider interlayer space, enabling enhanced solvent filtration permeability without  
236 compromising rejection efficiency thanks to the presence of numerous narrow slits  
237 within the membrane. The intercalation of stimuli-responsive polymers could allow the  
238 preparation of membranes with dynamic behavior. Proof of concept was demonstrated  
239 by Andreeva *et al.*, who reported the fabrication of a pH responsive membrane by  
240 strategically intercalated polyamine macromolecules (PA) into GO nanolaminates [50].  
241 The use of pH-responsive polymers introduces the capability to induce morphological  
242 changes within the nanochannels, leading to varied interlayer spacing in the complex  
243 membrane structure (Figure 2D). This responsive feature enables dynamic control over  
244 water transport, providing an environment-responsive functionality to the membrane.

245

246 Beyond separation properties, the interlayer spaces of nanochannels induce a  
247 confinement phenomenon at the nanometer level, which has profound consequences on  
248 the transport of molecules such as water. Both numerical simulation and experimental  
249 investigations have revealed that, under nanoconfined conditions between 2D  
250 nanosheets, water molecules exhibit remarkable structuring, forming orderly layers –  
251 typically one or several adjacent to the surface – while maintaining a disordered, bulk-  
252 like internal region. Calero *et al.* have determined the correlation between the structure  
253 of the water layer and the interlayer spacing in graphene slabs, revealing that optimal

254 slit-pore sizes at  $T = 275$  K are approximately  $6.5 \leq \omega/\text{\AA} \leq 7.0$  for a single layer,  $9.0 <$   
255  $\omega/\text{\AA} < 10.0$  for two layers, and  $12.5 < \omega/\text{\AA} < 14.0$  for three layers (Figure 3A) [98]. The  
256 water layer exhibits a higher density than that of bulk water [99], with water dipole  
257 orientations also undergoing notable alterations (Figure 3B) [100]. These orientation  
258 distributions are intimately tied to the strength of the confinement. Generally, the water  
259 dipoles in the interface layer preferentially orient parallel to the interior surface of the  
260 nanoconfinement, leading to a reconfiguration of hydrogen bonding networks. As the  
261 system reaches subnanometer confinement – wherein only a single layer of water is  
262 formed – the average hydrogen bond number sharply decreases (Figure 3C) [101].  
263 Monolayer water confined within nanochannels manifests 'ice-like' structures,  
264 exhibiting multiple shapes and patterns that are markedly influenced by the substrate  
265 material, such as square formations in graphene, rhombic in h-BN, and diamond shapes  
266 with isogonal tiling structures in MoS<sub>2</sub> [102,103]. Moreover, through adjustments of  
267 temperature and van der Waals pressure, monolayer water demonstrates various phase  
268 behaviors within the 2D slits, encompassing hexagonal, pentagonal, square, flat-  
269 rhombic, hexatic, superionic, and liquid phases (Figure 3D) [104].

270 The translational dynamics of water undergo notable alterations under  
271 nanoconfinement. Leoni *et al.* observed a substantial increase in water diffusion within  
272 sub-nanometer graphene slit pores, with rates surpassing those in bulk phases.  
273 Intriguingly, the longitudinal diffusion coefficient of water in graphene nanochannels  
274 is dependent on the slit size, reaching its maximum when the graphene plate separation  
275 distance measures  $8 \text{\AA}$  [101]. The hydrodynamics of water are also modified within  
276 nanoconfined spaces. While the slip length remains independent of the confinement  
277 size of the graphene slab [105], the viscosity of water is profoundly influenced by the  
278 layered structure of the confined water, especially when the capillary size is reduced to

279 less than 2 nm [106]. Notably, the shear viscosity of water is not only significantly  
280 augmented in subnanometer capillaries but also exhibits pronounced oscillations,  
281 emanating from commensurability between the channel size and the spatial requirement  
282 to accommodate a single layer of water molecules. Consequently, the synergistic effect  
283 of the ordered structure of nanoconfined water, the atomic smoothness, and electron  
284 distribution of the surface, coupled with the “frictionless” slip, translate to ultrafast  
285 water transport within graphene nanochannels.

286 When introducing oxygen-containing groups to the graphene basal planes, the  
287 capability to induce a layered structure under confinement is retained. The average  
288 distances between layers in GO laminates favor the creation of water layers distinct  
289 from those observed in graphene channels: 8.0 Å for a single layer, 9.3 Å for two layers  
290 and 11.7 Å for three layers of confined water, respectively [107]. The behavior also  
291 differs from the case on functionalization MoS<sub>2</sub> capillaries, for which the water  
292 structure is rapidly lost upon functionalization [62]. Within these confined layers, water  
293 density is typically larger than bulk [108]. However, the regular pattern of water  
294 molecules is disrupted by the presence of epoxide and hydroxide groups, translating to  
295 an increase in long-range disorder, especially evident within single-layer confined  
296 water [93]. Yet, a preference for the orientation of water dipoles remains, with a  
297 tendency towards a distribution parallel to the restricted direction [109].  
298 Simultaneously, the number of hydrogen bonds witnesses a notable reduction,  
299 particularly as confined water transitions from a two-layer to a single-layer  
300 configuration and is independent of the functional group arrangement on the graphene  
301 surface [107]. Contrasting with confinement between graphene slabs, the oxygen-  
302 containing group in GO nanosheets limits the flow of confined water, resulting in a  
303 reduced diffusion coefficient compared to bulk water. Furthermore, the axial shear

304 viscosities of water are heightened within 2D GO nanochannels, wherein the viscosity  
305 exhibits a declining pattern concomitant with increasing confinement [110].

306

307       Precise control over the interlayer spacing in nanolaminate membranes  
308 significantly influences the transport properties of solvent molecules and enhances  
309 separation performance by restricting ion and contaminant diffusion. Beyond the  
310 adjusting the architecture of these membranes, regulating the microenvironment also  
311 provides an efficient strategy for fine-tuning separation performance. This requires  
312 meticulous engineering of the membrane's composition, surface chemistry, and overall  
313 structure to achieve desired functionalities. In the following sections, we will discuss  
314 how modifications to the nanosheets adjust the physiochemical properties of the  
315 nanochannels in nanolaminates.

316

### 317       **Controlling the electrostatic interactions within the nanochannels**

318 Chemically exfoliated nanosheets, including positively charged layered double  
319 hydroxide (LDH), as well as negatively charged materials such as GO, TMDs, and  
320 MXene are the most studied 2D materials for nanolaminate membranes. The presence  
321 of charge excess carried by the nanosheets combined with the confined spaces within  
322 the interlayer gives rise to ion transport behavior governed by surface charge  
323 interactions [76,77]. When assembled into a nanolaminate membrane, negatively  
324 charged nanosheets facilitate faster transport of cations while blocking anions.  
325 Consequently, many 2D nanolaminate membranes can serve as cation/anion sieving  
326 membranes [78]. By modifying the nanosheets, it becomes possible to achieve  
327 reinforced charge distribution or reversed charge, leading to novel, tunable and efficient  
328 ion sieving performance in nanolaminate membranes. To neutralize the negative charge

329 of graphene oxide (GO), Zhang *et al.* employed 1-(3-Dimethylaminopropyl)-3-  
330 ethylcarbodiimide (EDC) to react with the carboxylic groups and subsequently graft  
331 branched polyethylenimine (PEI) through covalent coupling, resulting in GO  
332 nanosheets enriched with positive charges (p-GO) [79]. The p-GO membranes  
333 exhibited inhibited proton transport behavior compared to the pristine GO membrane.  
334 p-n heterojunctions consisting in n-GO and p-GO were found to generate an internal  
335 electric field, leading to salt-ion-blockade transport behavior [80]. By synergistically  
336 applying an external electric field, a depletion area is formed in the transition zone,  
337 resulting in significantly lower ionic concentration compared to the bulk phase.  
338 Deionized water could be extracted from the depletion zone, achieving a high rejection  
339 rate of 97.0% for NaCl and a water flux of  $1529 \text{ L m}^{-1} \text{ h}^{-1} \text{ bar}^{-1}$ . Yang *et al.* employed  
340 3-aminopropyl triethoxysilane (APTES) to functionalize MXene nanosheets *via* a  
341 silane coupling reaction, successfully synthesizing aminated MXene (AM-MXene)  
342 with a net positive charge [81]. Notably, the membranes formed by stacking AM-  
343 MXene nanosheets exhibited an anion-selective nanofluidic behavior, preferentially  
344 transporting  $\text{Cl}^-$  over  $\text{Na}^+$ . When utilized in osmotic power harvesting applications, this  
345 optimized membrane demonstrated a peak power density of  $10.98 \text{ W/m}^2$  under a natural  
346 salinity gradient, significantly outperforming the commercial benchmark of  $5 \text{ W/m}^2$ .

347 Noncovalent approaches involving the combination of polymers can be utilized to  
348 tune the surface charge of nanosheets. For instance, positively charged MXene  
349 nanosheets (p-MXene) were synthesized by adsorbing the positively charged polymer  
350 polydiallyl dimethyl ammonium (PDDA) onto the surface through electrostatic  
351 attraction [82]. The resulting p-MXene membrane exhibited excellent anion selectivity.  
352 Combining the p-MXene membrane with a pristine MXene membrane possessing  
353 cation selectivity, led to the creation of a heterogeneous MXene membrane with

354 asymmetric ionic diode behavior, thereby offering promising prospects as a high-  
355 performance osmotic power generator. Rather than reversing the surface charge, the  
356 same charged polymer can be used to enrich the surface charge of nanosheets through  
357 hydrogen bonding and van der Waals attraction. Zhang *et al.* employed negatively  
358 charged Kevlar nanofiber to modify the MXene nanosheets [49]. Assembling into a  
359 composite membrane led to an enhanced charge density in the nanochannels, resulting  
360 in increased cation selectivity. Consequently, this composite membrane exhibited  
361 superior osmotic power density when mixing river water and sea water.

362

### 363 **Controlling the chemical interactions within the nanochannels**

364 The interplay between contaminants and nanosheets plays a pivotal role in influencing  
365 the adsorption and diffusion of penetrants within the nanochannel. By incorporating  
366 various functional groups and molecules onto the basal plane of the nanosheets, the  
367 affinity of the nanochannel can be tailored, thereby tuning the separation properties. To  
368 illustrate this strategy, the following section will focus on controlling interactions inside  
369 nanochannels for gas separation and ion sieving.

370 Oxygen-containing groups present on the GO nanosheets not only create  
371 unobstructed nanochannels but also exhibit a stronger affinity for polar molecules such  
372 as CO<sub>2</sub> compared to N<sub>2</sub>. This strong adhesion between CO<sub>2</sub> and the oxygenated groups  
373 leads to preferential adsorption, thereby enhancing the CO<sub>2</sub> separation performance of  
374 GO membranes. To further enhance the oxygen content of GO nanosheets, Wang *et al.*  
375 employed poly(ethylene glycol) diamines (PEGDA) to covalently modify GO  
376 nanosheets by reacting with epoxy groups [83]. This modification enables the  
377 construction of CO<sub>2</sub>-philic nanodomains enriched with abundant oxygen-containing  
378 groups. Simultaneously, the unreacted GO surfaces exhibit weak adhesion to CO<sub>2</sub>,



379 facilitating low-friction diffusion, leading to excellent CO<sub>2</sub> separation performance.  
380 The strategy has been extended to other nanolaminate membranes, such as MXene.  
381 Zhang *et al.* intercalated PEGDA within the MXene interlayers to form heterogeneous  
382 nanochannels composed of both CO<sub>2</sub>-affinitive and non-CO<sub>2</sub>-affinitive nanodomains  
383 [84]. This rational architecture led to enhanced CO<sub>2</sub> separation efficiency (Figure 4A).  
384 In addition to oxygen groups, amino groups have also been employed to modify  
385 nanosheets and increase the affinity of the nanochannel. Zhou *et al.* grafted piperazine,  
386 an effective CO<sub>2</sub>-philic agent, onto GO nanosheets [85]. The grafted amine-brushes  
387 within the GO nanochannels facilitated the transport of CO<sub>2</sub> molecules, resulting in  
388 improved CO<sub>2</sub>/N<sub>2</sub> selectivity and CO<sub>2</sub> **permeance**.

389 Specific molecules like borates, ionic liquids or amino and carboxyl groups can  
390 create a favorable environment for CO<sub>2</sub> within the nanochannel [86-88]. The presence  
391 of ILs, which are characterized by nearly zero vapor pressure and high thermal and  
392 chemical stability, in the nanochannels induces strong interactions with CO<sub>2</sub>, bringing  
393 priority CO<sub>2</sub> transfer and inhibited N<sub>2</sub> permeance for the composite membrane, leading  
394 to improved CO<sub>2</sub> selectivity comparing with pristine nanolaminate membrane [89].

395 Controlling the affinity of nanochannels has additional advantages, particularly in  
396 enhancing ion sieving capabilities. Zhang *et al.* incorporated 1-butyldisulfonate-3-  
397 methylimidazolium, an ionic molecule, into the GO membrane (i-GO) [90]. This  
398 charged molecule not only establishes appropriate physical confinement through its  
399 ionic imidazole group but also fosters a favorable chemical environment for 2D ionic  
400 transport channels via its ionic sulfonic group. The presence of the ionic sulfonic groups  
401 in the i-GO membrane creates a hydrophilic environment, which boosts water affinity.  
402 This, in turn, ensures a high partition coefficient for K<sup>+</sup>, culminating in a significantly  
403 enhanced transport rate for monovalent ions. Lu *et al.* employed poly(sodium 4-styrene

404 sulfonate) (PSS) to intercalate into the 2D MXene nanolaminate membrane to achieve  
405 selective  $\text{Li}^+$  transport [91]. The modified membrane efficiently filters out  $\text{Li}^+$  from  
406 mixtures containing  $\text{Na}^+$ ,  $\text{K}^+$ , and  $\text{Mg}^{2+}$ . This high  $\text{Li}^+$  selectivity originates from precise  
407 interlayer spacing and the weak interaction between  $\text{Li}^+$  **and the sulfonate**  
408 **terminal ( $-\text{SO}_3^-$ )** (Figure 4B).

409

### 410 **Tuning the hydrophilicity of nanochannel**

411 The wettability of 2D nanolaminate membranes is determined by the surface properties  
412 of the nanosheets, which can easily be manipulated by tuning the surface chemistry of  
413 the nanosheets. Intercalated molecules residing within the nanochannels create  
414 hydrophilic or hydrophobic transport pathways. A hydrophobic nanochannel exhibits  
415 weak friction with water molecules due to their weak interaction, resulting in high water  
416 transport speeds. Conversely, a hydrophobic nanochannel restricts the entry of water  
417 molecules, whereas a hydrophilic nanochannel promotes water entry but hinders water  
418 transport due to strong adhesion interactions.

419 Graphene nanochannels with hydrophobic surfaces have demonstrated an  
420 exceptionally high water permeation rate due to their low hydraulic resistance [92].  
421 However, when graphene oxide (GO) nanochannels undergo oxidation, the presence of  
422 grafted oxygen groups on the nanosheets' surface significantly reduces the diffusion  
423 rate of water molecules by strongly absorbing them and impeding their movement [93].  
424 Unlike graphene nanochannels, which can be considered "frictionless" pathways for  
425 water transport, GO nanochannels exhibit a distinct parabolic velocity profile that  
426 indicates increased friction with water. The higher hydraulic resistance of GO  
427 membranes suppresses water shuttle and hampers efficient water permeation. To

428 leverage the potential of graphene nanochannels for ultra-fast water permeation, the  
429 concept of angstrom-channel graphene membranes (ACGMs) has been proposed by  
430 intercalating chitosan into thermally reduced graphene oxide (GO) sheets [94]. The  
431 hydrophobic ACGMs exhibited high flux for both water and organic solvents in  
432 pervaporation processes. Interestingly, when the feed solution consists of an ethanol  
433 and water mixture, the membranes prioritized water permeation over ethanol during  
434 pervaporation operations. Rather than reducing GO, Prabhakaran *et al.* enhanced its  
435 hydrophobicity by grafting imidazolium-based ionic liquids (ILs) onto its epoxide sites  
436 through a ring-opening reaction [43]. The longer alkyl chains attached to the  
437 imidazolium rings made the GO more hydrophobic. The adjustment optimizes water  
438 transport dynamics at the GO/IL interface, resulting in increased water flux. In addition  
439 to graphene and its derivatives, MoS<sub>2</sub> membranes with different grafted groups also  
440 exhibit varying surface wettability [62]. Hydrophobic groups, such as -CH<sub>3</sub> membranes  
441 lead to increased slip lengths when grafted on MoS<sub>2</sub> compared to the hydrophilic  
442 pristine MoS<sub>2</sub> nanosheets, resulting in higher water flux for membranes. Evidence of  
443 the reduced friction between the water molecule and the surface of the methyl  
444 functionalized MoS<sub>2</sub> nanosheets was provided by mapping the velocity of the confined  
445 water molecules between two MoS<sub>2</sub> slabs using molecular dynamic simulations (Figure  
446 5A). Water molecules were found to exhibit higher velocities on the methyl group,  
447 which was attributed to the screening of the electrostatic interactions between MoS<sub>2</sub>  
448 and the water molecules. This high-water flux makes hydrophobic membranes  
449 particularly advantageous for water permeation applications, similar in nature to the  
450 phenomena observed for hydrophobic systems such as carbon nanotubes and graphene.  
451 MXene laminated membranes possess hydrophilic nanochannels. Yet, by introducing  
452 poly(ionic liquid)s with readily exchangeable counter anions, their wettability can be

453 tuned (Figure 5B) [46]. Through straightforward anion exchange, the interlayer  
454 galleries transition from hydrophilic to more hydrophobic, doubling the water  
455 permeance.

456 In contrast to the high transport efficiency of hydrophobic nanochannels, hydrophilic  
457 nanochannels present advantages in antifouling and exhibit enhanced water-selective  
458 properties for membranes. Li *et al.* developed a zwitterionic polymer-brush-modified  
459 graphene oxide membrane featuring trimethylamine-N-oxide (TMAO) head groups  
460 [95]. This design created a strong surface hydration layer for the membrane. The  
461 hydrophilic surface and the disinfection effect provided by the quaternary ammonium  
462 groups both contribute to the T-GO membrane's impressive anti adhesion and contact  
463 inactivation abilities. Huang *et al.* were the first to discover that vermiculite laminates  
464 can be tuned from superhydrophilic to hydrophobic simply by intercalating hydrated  
465 cations into the membrane [96]. Lithium-intercalated vermiculite laminate (LiV-  
466 laminate) exhibits a zero contact angle under wet conditions. The super-hydrophilic  
467 surface of LiV-laminate originates from the anomalous hydrated structure of Li at the  
468 vermiculite surface. These super-hydrophilic membranes demonstrated excellent oil-  
469 water separation performance attributed to their outstanding antifouling property. Dai  
470 *et al.* introduced sodium polystyrene sulfonate (PSSNa) to create high-density  
471 hydrophilic microregions in the GO membrane [97]. These high-density ionized  
472 sulfonate groups within the polymer chains facilitate water sorption, enabling high-  
473 efficiency water-selective permeation. Simultaneously, the intercalation of polymer  
474 chains restricts swelling in the composite membrane due to robust  $\pi$ - $\pi$  interactions. The  
475 synergy between enhanced hydrophilicity and strict size confinement allows the  
476 PSSNa/GO membrane to exhibit superior separation performance in butanol  
477 pervaporation dehydration.

478

## 479 **Conclusions and outlook**

480 In the past decade, the field of membranes based on 2D materials has experienced  
481 remarkable growth, driven by the implementation of diverse chemical strategies to  
482 engineer the surface properties of these materials. This has paved the way for the  
483 creation of tailored 2D nanolaminate membranes with exceptional characteristics and  
484 functionalities. By precisely modifying the nanosheets, researchers have been able to  
485 assemble them into customizable nanochannels with controllable structures and  
486 favorable microenvironments. As a result, these chemically engineered nanolaminates  
487 have exhibited outstanding permeance and sieving performance across a wide range of  
488 applications, encompassing water desalination, nanofiltration, osmotic power  
489 harvesting, gas separation, and organic solvent dehydration. Despite the significant  
490 progress achieved in the fabrication of 2D material membranes, there still exist several  
491 challenges that demand attention to propel their further development (see Outstanding  
492 Questions):

493 *(1) Advancing the functionalization strategies for 2D Nanosheets:* Over the years,  
494 numerous functionalization strategies have been successfully adapted for the  
495 modification of 2D nanosheets. However, the achievement of a controllable degree of  
496 functionalization remains to be explored. The existence of different functionalization  
497 contents, coupled with uneven size distributions and varying layer numbers of 2D  
498 nanosheets, poses a significant challenge for 2D material membranes. Addressing this  
499 challenge holds importance as it can unlock the full potential of 2D nanosheets for  
500 various applications. Achieving uniformity in the degree of functionalization and  
501 controlling the distribution of functional groups across the nanosheet surface are crucial  
502 factors in enhancing the repeatability of 2D material membranes. Such advancements

503 will not only ensure reliable and consistent performance but also enable the  
504 reproducibility of experimental results across the different research groups.

505 (2) *Understanding the role of decorated molecules or groups:* The assembly of  
506 modified nanosheets into membranes offers remarkable opportunities to achieve  
507 tunable architectures and regulated microenvironments. However, a comprehensive  
508 understanding of how the surface chemistry of the nanochannels affects the transport  
509 of targeted penetrants is still lacking. It is imperative that future research efforts are  
510 dedicated to addressing this knowledge gap. Gaining insights into the intricate  
511 interactions between the surface functional groups and the transport of penetrants  
512 within the nanochannels holds significant implications for the optimization of 2D  
513 material membranes. This could be addressed by the development of theoretical models  
514 that can elucidate the underlying mechanisms governing the influence of functional  
515 groups on penetrant transport.

516 (3) *Generating a synergistic relationship between the nanostructure and the surface*  
517 *physicochemical properties:* Considerable progress has been made in understanding the  
518 impact of nanostructure and surface physicochemical properties on the performance of  
519 separation membranes. Existing studies have primarily focused on two aspects: the  
520 tunability of channel size to achieve physical separation confinement and the regulation  
521 of surface physicochemical properties to prioritize the transport of penetrants. However,  
522 a comprehensive approach that combines both aspects, encompassing the synergistic  
523 regulation of interlayer space and controlled surface physicochemical properties  
524 through modification, is essential to fully exploit the potential of physical and chemical  
525 separation mechanisms for the development of highly efficient separation membranes.

526

527

528 **Acknowledgments**

529 D.V. and W.W. acknowledge funding from the European Research Council (ERC)  
530 under the European Union's Horizon 2020 research and innovation programme (grant  
531 agreement no. 804320). W.W. acknowledge Ph.D. scholarship from the China  
532 Scholarship Council (CSC). D.V. and C.S. acknowledge funding from the French  
533 National Agency (ANR, programme 2D-MEMBA, ANR-21-CE09-0034-01). C.S.  
534 acknowledges funding from the French National Agency (ANR, JCJC programme,  
535 MONOMEANR-20-CE08-0009).

536

537 **References**

- 538 1. Werber, J.R. *et al.* (2016) Materials for next-generation desalination and water  
539 purification membranes. *Nature Reviews Materials* 1, 1-15
- 540 2. Koros, W.J. and Zhang, C. (2017) Materials for next-generation molecularly  
541 selective synthetic membranes. *Nature materials* 16, 289-297
- 542 3. Park, H.B. *et al.* (2017) Maximizing the right stuff: The trade-off between  
543 membrane permeability and selectivity. *Science* 356,
- 544 4. White, L.S. (2020) Effect of operating environment on membrane performance.  
545 *Current Opinion in Chemical Engineering* 28, 105-111
- 546 5. Liu, P. *et al.* (2020) Two-dimensional material membranes for critical  
547 separations. *Inorganic Chemistry Frontiers* 7, 2560-2581
- 548 6. Kang, Y. *et al.* (2019) 2D laminar membranes for selective water and ion  
549 transport. *Advanced Functional Materials* 29, 1902014
- 550 7. Zhang, H. (2018) Introduction: 2D materials chemistry. *Chemical reviews* 118,  
551 6089-6090
- 552 8. Tan, C. *et al.* (2017) Recent advances in ultrathin two-dimensional  
553 nanomaterials. *Chemical reviews* 117, 6225-6331
- 554 9. Xu, G.-R. *et al.* (2019) Two-dimensional (2D) nanoporous membranes with  
555 sub-nanopores in reverse osmosis desalination: Latest developments and future

- 556 directions. *Desalination* 451, 18-34
- 557 10. Jian, M. *et al.* (2020) Ultrathin water-stable metal-organic framework  
558 membranes for ion separation. *Science advances* 6, eaay3998
- 559 11. Wang, Z. *et al.* (2020) Covalent organic frameworks for separation applications.  
560 *Chemical Society Reviews* 49, 708-735
- 561 12. Kumar, P. *et al.* (2020) One-dimensional intergrowths in two-dimensional  
562 zeolite nanosheets and their effect on ultra-selective transport. *Nature materials*  
563 19, 443-449
- 564 13. Yang, J. *et al.* (2022) Advancing osmotic power generation by covalent organic  
565 framework monolayer. *Nature nanotechnology* 17, 622-628
- 566 14. Yang, Y. *et al.* (2019) Large-area graphene-nanomesh/carbon-nanotube hybrid  
567 membranes for ionic and molecular nanofiltration. *Science* 364, 1057-1062
- 568 15. Feng, J. *et al.* (2016) Single-layer MoS<sub>2</sub> nanopores as nanopower generators.  
569 *Nature* 536, 197-200
- 570 16. Cheng, C. *et al.* (2021) Molecular size-dependent subcontinuum solvent  
571 permeation and ultrafast nanofiltration across nanoporous graphene  
572 membranes. *Nature Nanotechnology* 16, 989-995
- 573 17. Wang, S. *et al.* (2020) Two-dimensional nanochannel membranes for molecular  
574 and ionic separations. *Chemical Society Reviews* 49, 1071-1089
- 575 18. Cheng, L. *et al.* (2021) Two-dimensional-material membranes: manipulating  
576 the transport pathway for molecular separation. *Accounts of Materials Research*  
577 2, 114-128
- 578 19. Cai, X. *et al.* (2018) Preparation of 2D material dispersions and their  
579 applications. *Chemical Society Reviews* 47, 6224-6266
- 580 20. Zhu, M. *et al.* (2013) Fluorographene nanosheets with broad solvent  
581 dispersibility and their applications as a modified layer in organic field-effect  
582 transistors. *Physical Chemistry Chemical Physics* 15, 20992-21000
- 583 21. Hartmann, S.J. *et al.* (2020) Electrochemical properties of nitrogen and oxygen  
584 doped reduced graphene oxide. *Energies* 13, 312
- 585 22. Lei, W. *et al.* (2015) Boron nitride colloidal solutions, ultralight aerogels and  
586 freestanding membranes through one-step exfoliation and functionalization.  
587 *Nature communications* 6, 1-8
- 588 23. Liu, L. *et al.* (2023) Tuning the surface chemistry of MXene to improve energy



- 589 storage: example of nitrification by salt melt. *Advanced Energy Materials* 13,  
590 2202709
- 591 24. Chen, C. *et al.* (2018) Functionalized boron nitride membranes with ultrafast  
592 solvent transport performance for molecular separation. *Nature*  
593 *communications* 9, 1902
- 594 25. Hidayah, N. *et al.* (2020) Roles of linear alkyl chain alkylation on reinforcement  
595 of graphene based polypropylene nanocomposites. *Materials Today*  
596 *Communications* 22, 100775
- 597 26. Voiry, D. *et al.* (2015) Covalent functionalization of monolayered transition  
598 metal dichalcogenides by phase engineering. *Nature chemistry* 7, 45-49
- 599 27. de los Reyes, C.A. *et al.* (2019) Tunable Alkylation of White Graphene  
600 (Hexagonal Boron Nitride) Using Reductive Conditions. *The Journal of*  
601 *Physical Chemistry C* 123, 19725-19733
- 602 28. Jing, H. *et al.* (2021) Modulation of the electronic properties of MXene (Ti<sub>3</sub>C<sub>2</sub>T<sub>x</sub>)  
603 via surface-covalent functionalization with diazonium. *ACS nano* 15, 1388-  
604 1396
- 605 29. Jia, Z. and Wang, Y. (2015) Covalently crosslinked graphene oxide membranes  
606 by esterification reactions for ions separation. *Journal of Materials Chemistry*  
607 *A* 3, 4405-4412
- 608 30. Meng, N. *et al.* (2018) A low-pressure GO nanofiltration membrane crosslinked  
609 via ethylenediamine. *Journal of Membrane Science* 548, 363-371
- 610 31. Chen, L. *et al.* (2017) Ion sieving in graphene oxide membranes via cationic  
611 control of interlayer spacing. *Nature* 550, 380-383
- 612 32. Chuah, C.Y. *et al.* (2020) The influence of cations intercalated in graphene  
613 oxide membranes in tuning H<sub>2</sub>/CO<sub>2</sub> separation performance. *Separation and*  
614 *Purification Technology* 246, 116933
- 615 33. Wang, J. *et al.* (2020) Ion sieving by a two-dimensional Ti<sub>3</sub>C<sub>2</sub>T<sub>x</sub> alginate  
616 lamellar membrane with stable interlayer spacing. *Nature communications* 11,  
617 1-10
- 618 34. Fan, Y. *et al.* (2021) Nickel (II) ion-intercalated MXene membranes for  
619 enhanced H<sub>2</sub>/CO<sub>2</sub> separation. *Frontiers of Chemical Science and Engineering*  
620 15, 882-891
- 621 35. Nie, L. *et al.* (2020) Realizing small-flake graphene oxide membranes for

- 622 ultrafast size-dependent organic solvent nanofiltration. *Science Advances* 6,  
623 eaaz9184
- 624 36. Yuan, S. *et al.* (2021) Stable cation-controlled reduced graphene oxide  
625 membranes for improved NaCl rejection. *Journal of Membrane Science* 621,  
626 118995
- 627 37. Chu, C. *et al.* (2020) Precise ångström controlling the interlayer channel of  
628 MoS<sub>2</sub> membranes by cation intercalation. *Journal of Membrane Science* 615,  
629 118520
- 630 38. Ding, L. *et al.* (2020) Effective ion sieving with Ti<sub>3</sub>C<sub>2</sub>T<sub>x</sub> MXene membranes  
631 for production of drinking water from seawater. *Nature Sustainability* 3, 296-  
632 302
- 633 39. Guan, K. *et al.* (2021) Chemically converted graphene nanosheets for the  
634 construction of ion-exclusion nanochannel membranes. *Nano Letters* 21, 3495-  
635 3502
- 636 40. Kim, H.J. *et al.* (2016) Reverse osmosis nanocomposite membranes containing  
637 graphene oxides coated by tannic acid with chlorine-tolerant and antimicrobial  
638 properties. *Journal of Membrane Science* 514, 25-34
- 639 41. Chen, D. *et al.* (2017) Enhanced gas separation through nanoconfined ionic  
640 liquid in laminated MoS<sub>2</sub> membrane. *ACS applied materials & interfaces* 9,  
641 44251-44257
- 642 42. Ying, W. *et al.* (2018) Ionic liquid selectively facilitates CO<sub>2</sub> transport through  
643 graphene oxide membrane. *ACS nano* 12, 5385-5393
- 644 43. Tan, S. *et al.* (2022) Tuning the Charge and Hydrophobicity of Graphene Oxide  
645 Membranes by Functionalization with Ionic Liquids at Epoxide Sites. *ACS*  
646 *Applied Materials & Interfaces* 14, 19031-19042
- 647 44. Hu, Y. *et al.* (2023) Confined Ionic-Liquid-Mediated Cation Diffusion through  
648 Layered Membranes for High-Performance Osmotic Energy Conversion.  
649 *Advanced Materials*, 2301285
- 650 45. Niu, Z. *et al.* (2022) Nanoconfined CO<sub>2</sub>-philic ionic liquid in laminated g-C<sub>3</sub>N<sub>4</sub>  
651 membrane for the highly efficient separation of CO<sub>2</sub>. *Separation and*  
652 *Purification Technology* 297, 121513
- 653 46. Yi, M. *et al.* (2022) Poly (ionic liquid)-Armored MXene Membrane: Interlayer  
654 Engineering for Facilitated Water Transport. *Angewandte Chemie* 134,

- 655 e202202515
- 656 47. Shao, D.-D. *et al.* (2021) Enhancing interfacial adhesion of MXene  
657 nanofiltration membranes via pillaring carbon nanotubes for pressure and  
658 solvent stable molecular sieving. *Journal of Membrane Science* 623, 119033
- 659 48. Sun, Y. *et al.* (2021) Assembly of multidimensional MXene-carbon nanotube  
660 ultrathin membranes with an enhanced anti-swelling property for water  
661 purification. *Journal of Membrane Science* 623, 119075
- 662 49. Zhang, Z. *et al.* (2019) Mechanically strong MXene/Kevlar nanofiber  
663 composite membranes as high-performance nanofluidic osmotic power  
664 generators. *Nature communications* 10, 1-9
- 665 50. Andreeva, D.V. *et al.* (2021) Two-dimensional adaptive membranes with  
666 programmable water and ionic channels. *Nature Nanotechnology* 16, 174-180
- 667 51. Dong, L. *et al.* (2020) NH<sub>2</sub>-Fe<sub>3</sub>O<sub>4</sub>-regulated graphene oxide membranes with  
668 well-defined laminar nanochannels for desalination of dye solutions.  
669 *Desalination* 476, 114227
- 670 52. Wang, S. *et al.* (2019) 2D-dual-spacing channel membranes for high  
671 performance organic solvent nanofiltration. *Journal of Materials Chemistry A*  
672 7, 11673-11682
- 673 53. Long, Q. *et al.* (2021) Self-assembly enabled nano-intercalation for stable high-  
674 performance MXene membranes. *Journal of Membrane Science*, 119464
- 675 54. Secchi, E. *et al.* (2016) Massive radius-dependent flow slippage in carbon  
676 nanotubes. *Nature* 537, 210-213
- 677 55. Radha, B. *et al.* (2016) Molecular transport through capillaries made with  
678 atomic-scale precision. *Nature* 538, 222-225
- 679 56. Kavokine, N. *et al.* (2022) Fluctuation-induced quantum friction in nanoscale  
680 water flows. *Nature* 602, 84-90
- 681 57. Li, H. *et al.* (2013) Ultrathin, molecular-sieving graphene oxide membranes for  
682 selective hydrogen separation. *Science* 342, 95-98
- 683 58. Wei, N. *et al.* (2014) Breakdown of fast water transport in graphene oxides.  
684 *Physical Review E* 89, 012113
- 685 59. Mouhat, F. *et al.* (2020) Structure and chemistry of graphene oxide in liquid  
686 water from first principles. *Nature communications* 11, 1566
- 687 60. Abraham, J. *et al.* (2017) Tunable sieving of ions using graphene oxide

- 688 membranes. *Nature nanotechnology* 12, 546-550
- 689 61. Wang, Z. *et al.* (2017) Understanding the aqueous stability and filtration  
690 capability of MoS<sub>2</sub> membranes. *Nano letters* 17, 7289-7298
- 691 62. Ries, L. *et al.* (2019) Enhanced sieving from exfoliated MoS<sub>2</sub> membranes via  
692 covalent functionalization. *Nature materials* 18, 1112-1117
- 693 63. Wang, W. *et al.* (2023) High-surface-area functionalized nanolaminated  
694 membranes for energy-efficient nanofiltration and desalination in forward  
695 osmosis. *Nature Water* 1, 187-197
- 696 64. Mei, L. *et al.* (2022) Simultaneous electrochemical exfoliation and covalent  
697 functionalization of MoS<sub>2</sub> membrane for ion sieving. *Advanced Materials* 34,  
698 2201416
- 699 65. Hoenig, E. *et al.* (2020) Controlling the Structure of MoS<sub>2</sub> Membranes via  
700 Covalent Functionalization with Molecular Spacers. *Nano Letters* 20, 7844-  
701 7851
- 702 66. Ding, L. *et al.* (2018) MXene molecular sieving membranes for highly efficient  
703 gas separation. *Nature communications* 9, 1-7
- 704 67. Wu, X. *et al.* (2019) Elucidating ultrafast molecular permeation through well-  
705 defined 2D nanochannels of lamellar membranes. *Angewandte Chemie* 131,  
706 18695-18700
- 707 68. Hung, W.-S. *et al.* (2014) Cross-linking with diamine monomers to prepare  
708 composite graphene oxide-framework membranes with varying d-spacing.  
709 *Chemistry of Materials* 26, 2983-2990
- 710 69. Jia, Z. *et al.* (2016) Diamines cross-linked graphene oxide free-standing  
711 membranes for ion dialysis separation. *Journal of Membrane Science* 520, 139-  
712 144
- 713 70. Zhou, H. *et al.* (2023) Cross-Linked and Doped Graphene Oxide Membranes  
714 with Excellent Antifouling Capacity for Rejection of Antibiotics and Salts. *ACS*  
715 *Applied Materials & Interfaces* 15, 8636-8652
- 716 71. Guan, K. *et al.* (2022) Integration of thin film composite graphene oxide  
717 membranes for solvent resistant nanofiltration. *Journal of Membrane Science*  
718 660, 120861
- 719 72. Austria, H.F.M. *et al.* (2023) Tailoring the specific crosslinking sites of  
720 graphene oxide framework nanosheets for controlled nanofiltration of salts and

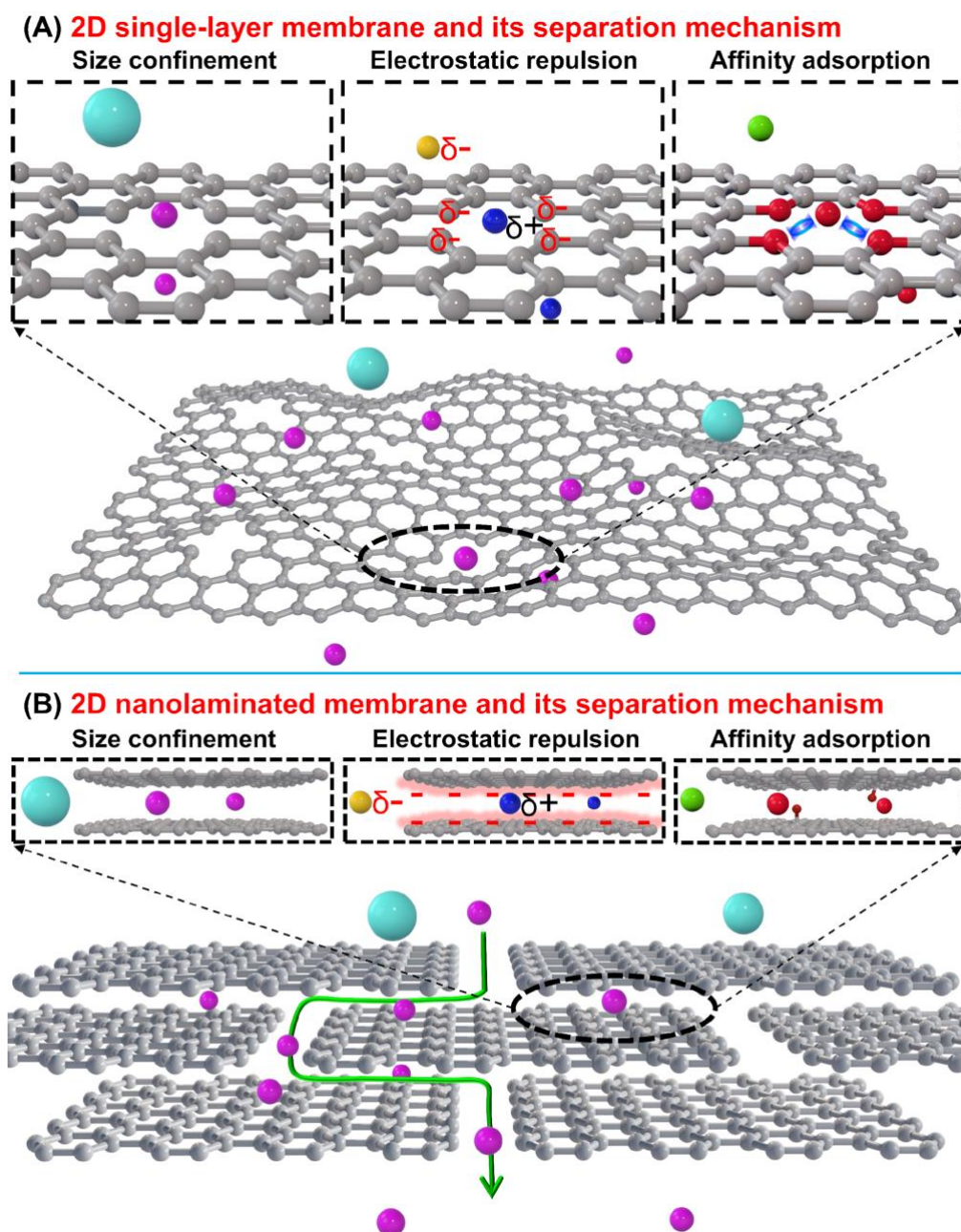
- 721 dyes. *Journal of Cleaner Production* 395, 136280
- 722 73. Zhang, Y. *et al.* (2017) Thermally evolved and boron bridged graphene oxide  
723 (GO) frameworks constructed on microporous hollow fiber substrates for water  
724 and organic matters separation. *Carbon* 123, 193-204
- 725 74. Pandey, R.P. *et al.* (2022) Cross-linked laminar graphene oxide membranes for  
726 wastewater treatment and desalination: A review. *Journal of Environmental*  
727 *Management* 317, 115367
- 728 75. Zhu, J. *et al.* (2020) Precisely Tunable Ion Sieving with an Al<sub>13</sub>-Ti<sub>3C<sub>2</sub>T<sub>x</sub></sub>
- 729 Lamellar Membrane by Controlling Interlayer Spacing. *ACS nano* 14, 15306-  
730 15316
- 731 76. Wu, Y. *et al.* (2021) Surface Charge Regulated Asymmetric Ion Transport in  
732 Nanoconfined Space. *Small*, 2101099
- 733 77. Xie, L. *et al.* (2023) Surface Charge Modification on 2D Nanofluidic Membrane  
734 for Regulating Ion Transport. *Advanced Functional Materials* 33, 2208959
- 735 78. Ji, J. *et al.* (2017) Osmotic power generation with positively and negatively  
736 charged 2D nanofluidic membrane pairs. *Advanced Functional Materials* 27,  
737 1603623
- 738 79. Zhang, X. *et al.* (2019) Asymmetric electrokinetic proton transport through 2D  
739 nanofluidic heterojunctions. *ACS nano* 13, 4238-4245
- 740 80. Wen, Q. *et al.* (2020) Electric-Field-Induced Ionic Sieving at Planar Graphene  
741 Oxide Heterojunctions for Miniaturized Water Desalination. *Advanced*  
742 *Materials* 32, 1903954
- 743 81. Wang, S. *et al.* (2023) Toward explicit anion transport nanochannels for osmotic  
744 power energy using positive charged MXene membrane via amination strategy.  
745 *Journal of Membrane Science* 668, 121203
- 746 82. Ding, L. *et al.* (2022) Bioinspired Ti<sub>3C<sub>2</sub>T<sub>x</sub></sub> MXene-Based Ionic Diode  
747 Membrane for High-Efficient Osmotic Energy Conversion. *Angewandte*  
748 *Chemie International Edition* 61, e202206152
- 749 83. Wang, S. *et al.* (2017) Graphene oxide membranes with heterogeneous  
750 nanodomains for efficient CO<sub>2</sub> separations. *Angewandte Chemie International*  
751 *Edition* 56, 14246-14251
- 752 84. Zhang, Y. *et al.* (2023) Rational Design of MXene Hollow Fiber Membranes  
753 for Gas Separations. *Nano Letters* 23, 2710-2718

- 754 85. Zhou, F. *et al.* (2017) Ultrathin graphene oxide-based hollow fiber membranes  
755 with brush-like CO<sub>2</sub>-philic agent for highly efficient CO<sub>2</sub> capture. *Nature*  
756 *communications* 8, 1-8
- 757 86. Shen, J. *et al.* (2018) 2D MXene nanofilms with tunable gas transport channels.  
758 *Advanced Functional Materials* 28, 1801511
- 759 87. Wang, S. *et al.* (2016) A highly permeable graphene oxide membrane with fast  
760 and selective transport nanochannels for efficient carbon capture. *Energy &*  
761 *Environmental Science* 9, 3107-3112
- 762 88. Zhao, R. *et al.* (2022) Vermiculite membranes intercalated with amino acids for  
763 efficient biogas upgrading. *Separation and Purification Technology* 297,  
764 121465
- 765 89. Jia, Y. *et al.* (2022) Facile ionization of the nanochannels of lamellar  
766 membranes for stable ionic liquid immobilization and efficient CO<sub>2</sub> separation.  
767 *ACS nano* 16, 14379-14389
- 768 90. Zhang, M. *et al.* (2021) Designing biomimic two-dimensional ionic transport  
769 channels for efficient ion sieving. *ACS nano* 15, 5209-5220
- 770 91. Lu, Z. *et al.* (2021) A lamellar MXene (Ti<sub>3</sub>C<sub>2</sub>T<sub>x</sub>)/PSS composite membrane  
771 for fast and selective lithium-ion separation. *Angewandte Chemie* 133, 22439-  
772 22443
- 773 92. Xie, Q. *et al.* (2018) Fast water transport in graphene nanofluidic channels.  
774 *Nature nanotechnology* 13, 238-245
- 775 93. Zheng, S. *et al.* (2017) Swelling of graphene oxide membranes in aqueous  
776 solution: characterization of interlayer spacing and insight into water transport  
777 mechanisms. *ACS nano* 11, 6440-6450
- 778 94. Chen, X. *et al.* (2020) Selective Permeation of Water through Angstrom-  
779 Channel Graphene Membranes for Bioethanol Concentration. *Advanced*  
780 *Materials* 32, 2002320
- 781 95. Li, M. *et al.* (2021) Graphene oxide nanofiltration membrane with  
782 trimethylamine-N-oxide zwitterions for robust biofouling resistance. *Journal of*  
783 *Membrane Science* 640, 119855
- 784 96. Huang, K. *et al.* (2020) Cation-controlled wetting properties of vermiculite  
785 membranes and its promise for fouling resistant oil–water separation. *Nature*  
786 *communications* 11, 1-10

- 787 97. Dai, L. *et al.* (2023) Two-dimensional confined channels with high-density  
788 hydrophilic microregions for enhanced selective water transport. *Journal of*  
789 *Membrane Science* 671, 121398
- 790 98. Calero, C. and Franzese, G. (2020) Water under extreme confinement in  
791 graphene: Oscillatory dynamics, structure, and hydration pressure explained as  
792 a function of the confinement width. *Journal of Molecular Liquids* 317, 114027
- 793 99. Zhao, Z. *et al.* (2022) Giant mechanocaloric effect of nanoconfined water near  
794 room temperature. *Cell Reports Physical Science* 3,
- 795 100. Ruiz-Barragan, S. *et al.* (2018) Nanoconfined water within graphene slit pores  
796 adopts distinct confinement-dependent regimes. *The journal of physical*  
797 *chemistry letters* 10, 329-334
- 798 101. Leoni, F. *et al.* (2021) Nanoconfined fluids: Uniqueness of water compared to  
799 other liquids. *ACS nano* 15, 19864-19876
- 800 102. Trushin, M. *et al.* (2023) Two-dimensional non-linear hydrodynamics and  
801 nanofluidics. *Communications Physics* 6, 162
- 802 103. Kwac, K. *et al.* (2017) Multilayer two-dimensional water structure confined in  
803 MoS<sub>2</sub>. *The Journal of Physical Chemistry C* 121, 16021-16028
- 804 104. Kapil, V. *et al.* (2022) The first-principles phase diagram of monolayer  
805 nanoconfined water. *Nature* 609, 512-516
- 806 105. Falk, K. *et al.* (2010) Molecular origin of fast water transport in carbon nanotube  
807 membranes: superlubricity versus curvature dependent friction. *Nano letters* 10,  
808 4067-4073
- 809 106. Neek-Amal, M. *et al.* (2016) Commensurability effects in viscosity of  
810 nanoconfined water. *ACS nano* 10, 3685-3692
- 811 107. Meshhal, M. and Kühn, O. (2022) Diffusion of Water Confined between  
812 Graphene Oxide Layers: Implications for Membrane Filtration. *ACS Applied*  
813 *Nano Materials* 5, 11119-11128
- 814 108. Tan, Q. *et al.* (2022) Effects of interlayer spacing and oxidation degree of  
815 graphene oxide nanosheets on water permeation: a molecular dynamics study.  
816 *Journal of Molecular Modeling* 28, 57
- 817 109. Ayappa, K.G. (2019) Enhancing the Dynamics of Water Confined between  
818 Graphene Oxide Surfaces with Janus Interfaces: A Molecular Dynamics Study.  
819 *The journal of physical chemistry. B* 123, 2978-2993

820 110. Chen, Y. *et al.* (2020) Viscosity and structure of water and ethanol within GO  
821 nanochannels: A molecular simulation study. *The Journal of Physical*  
822 *Chemistry B* 124, 10961-10970  
823  
824  
825

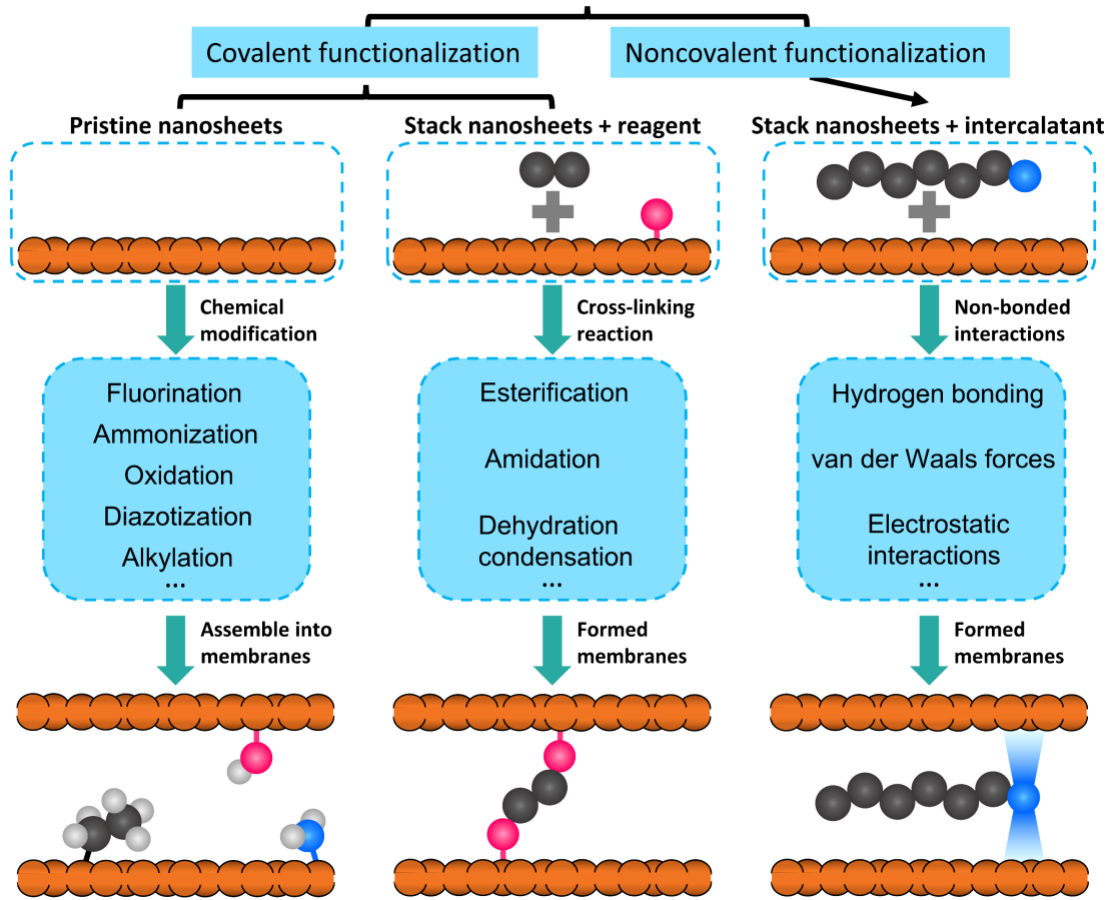




826

827 **Figure 1.** Schematic diagram of two types of selective channels constructed by 2D  
 828 materials and their separation mechanism. (A) 2D single-layer membranes. The  
 829 selectivity originates from the size confinement, electrostatic interaction and chemical  
 830 or physical adsorption of nanopores for the penetrants. (B) 2D nanolaminate  
 831 membranes. The selectivity comes from the sized exclusion, electrostatic repulsion and  
 832 prior adsorption of nanochannels for the penetrants.

## Modification methods of 2D nanosheets for nanolaminate membranes



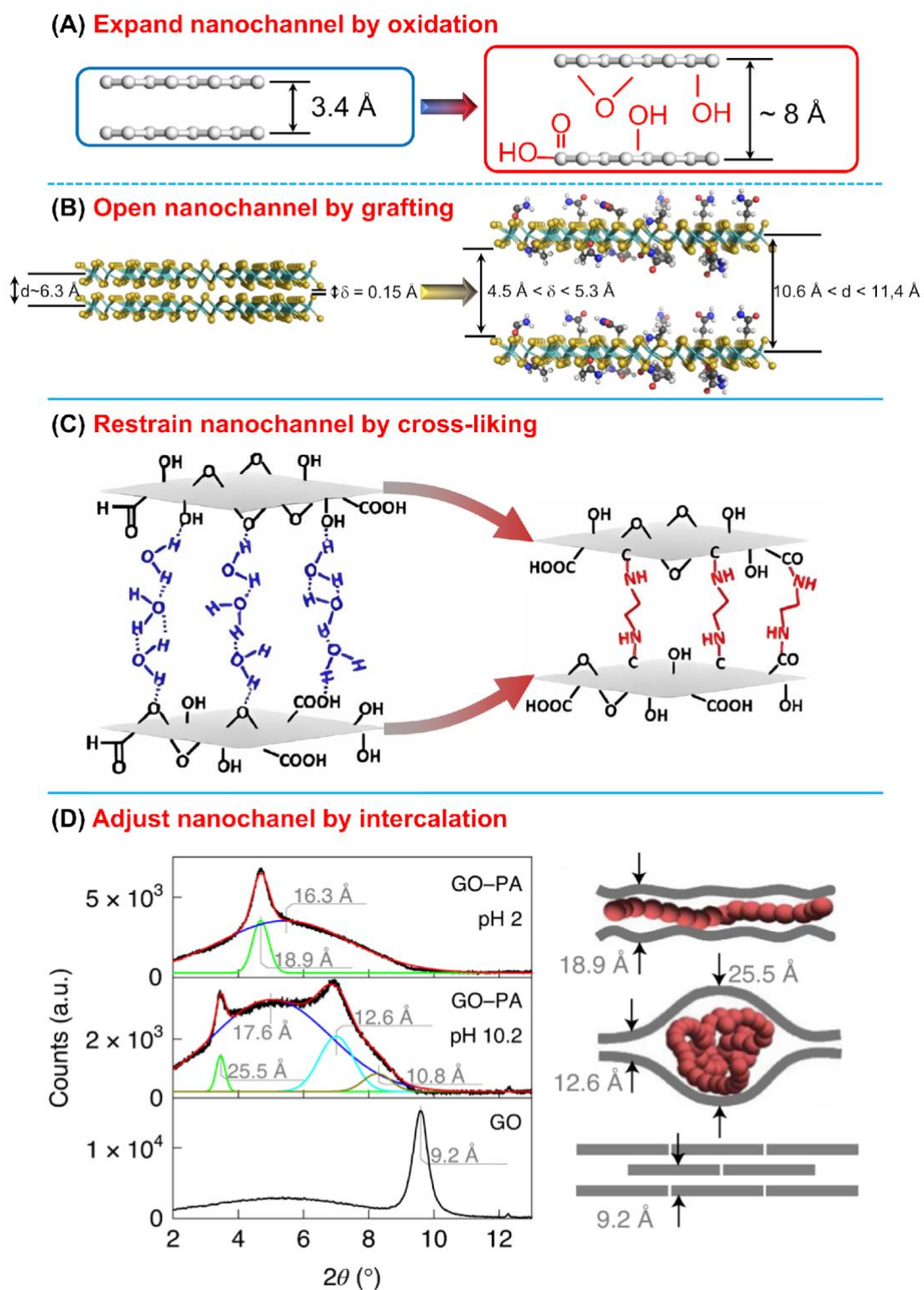
833

834 **Figure I.** The nanosheets modification strategies employed in 2D nanolaminate

835 membranes.

836

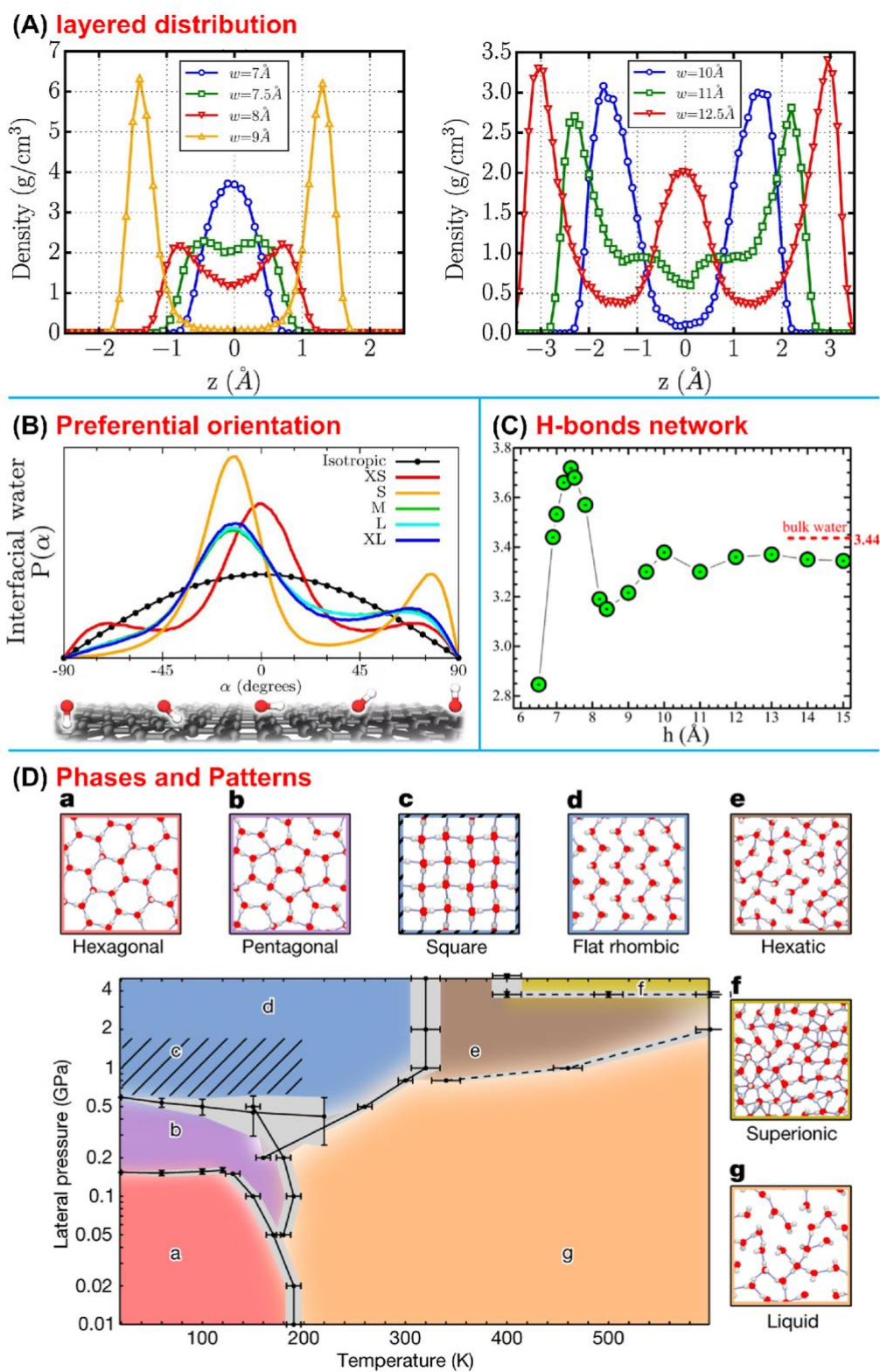
837



839

840 **Figure 2.** The interlayer space changes of 2D nanolaminated membranes aroused by  
 841 covalent or non-covalent modification. (A) Schematic illustration of d-spacings of

842 graphene and GO nanochannel. **(B)** Schematics of restacked pristine MoS<sub>2</sub> and  
843 functionalized MoS<sub>2</sub> nanosheets with the interlayer spacing  $d$  and the capillary width  $\delta$ .  
844 **(C)** Structural diagram and  $d$ -spacing of wet GO and diamine monomer cross-linked  
845 GO membrane. **(D)** X-ray reflection spectra for the GO-PA membranes prepared at  
846 different PH solutions with extracted interlayer distances (left) and schematic  
847 illustrations for the membranes' structure (right). Images adapted, with permission,  
848 from [31,50,62,66,68,93].  
849



850

851 **Figure 3.** The structure of nanoconfined water under 2D nanochannel. (A) Water

852 density distribution at different graphene-plate distances ( $w$ ). (B) Orientation

853 distribution of of interfacial layer water under confinement. (C) Evolution of the

854 average number of hydrogen bonds per molecule as a function of nanochannel height  $h$

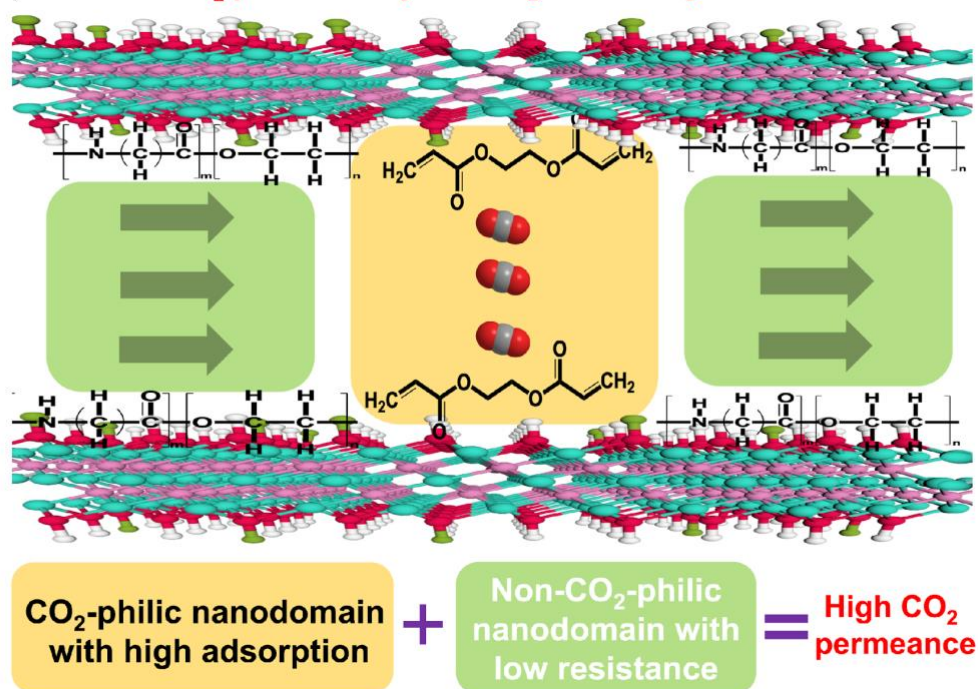
855 in the confined subvolume. **(D)** Phase diagram of monolayer nanoconfined water.

856 Images adapted, with permission, from [98,100,101,104,106].

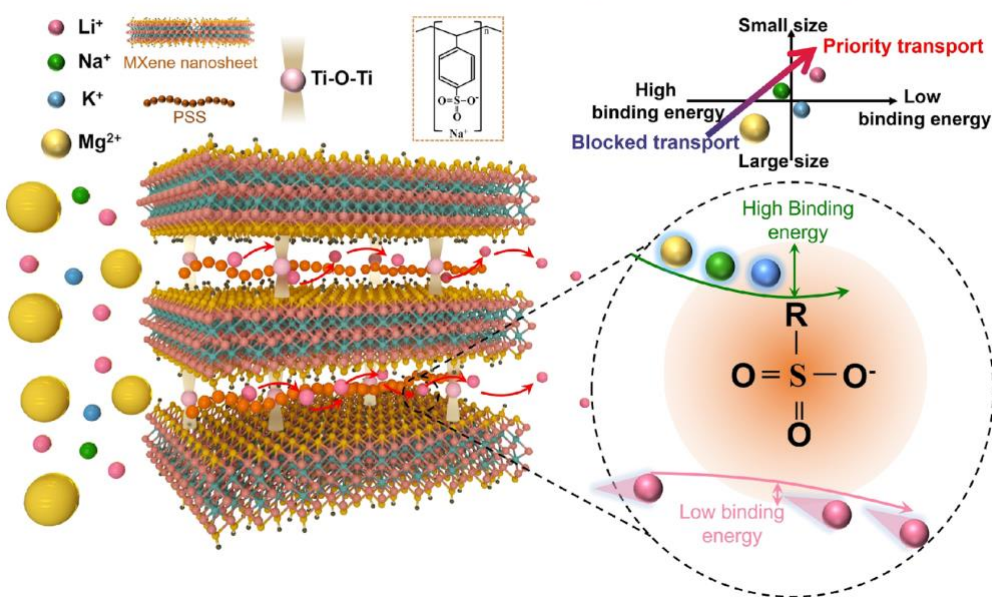
857

858

(A) Facilitate CO<sub>2</sub> permeance by tailoring the affinity



(B) Selectively screen ions by introducing chemical binding site



859

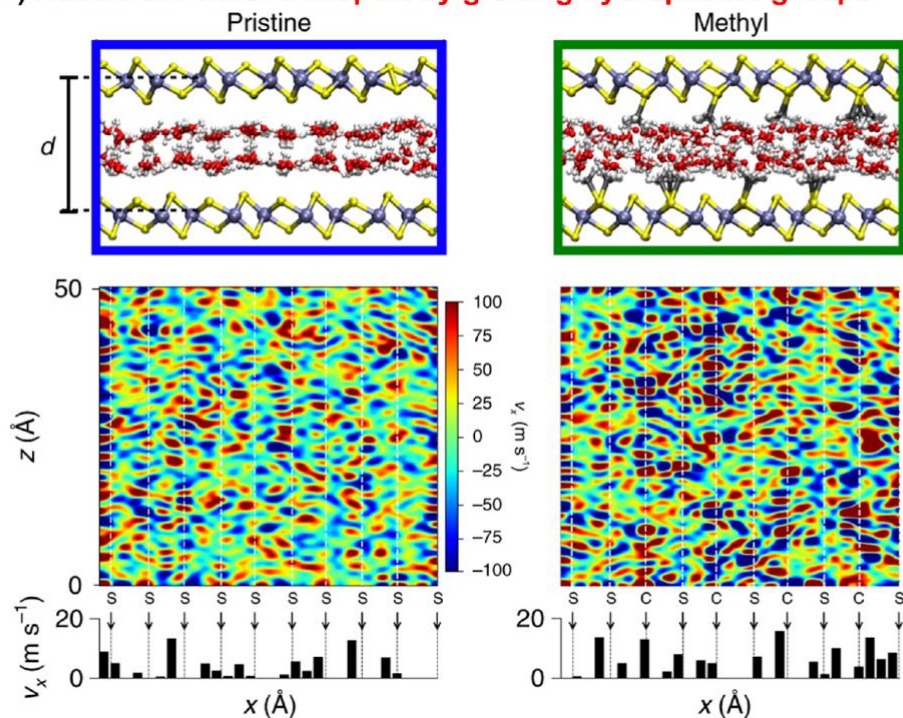
860 **Figure 4.** The nanochannel affinity adjustment of 2D nanolaminated membrane based  
861 on the chemical modification. (A) Representation of gas molecules transport in the  
862 MXene stacking membranes channels containing both CO<sub>2</sub>-philic and non-CO<sub>2</sub>-philic  
863 nanodomains. (B) Schematic diagram of the rapid transport subnanochannels for Li<sup>+</sup> in  
864 MXene/PSS composite membranes. Images adapted, with permission, from

865 [84,85,89,91].

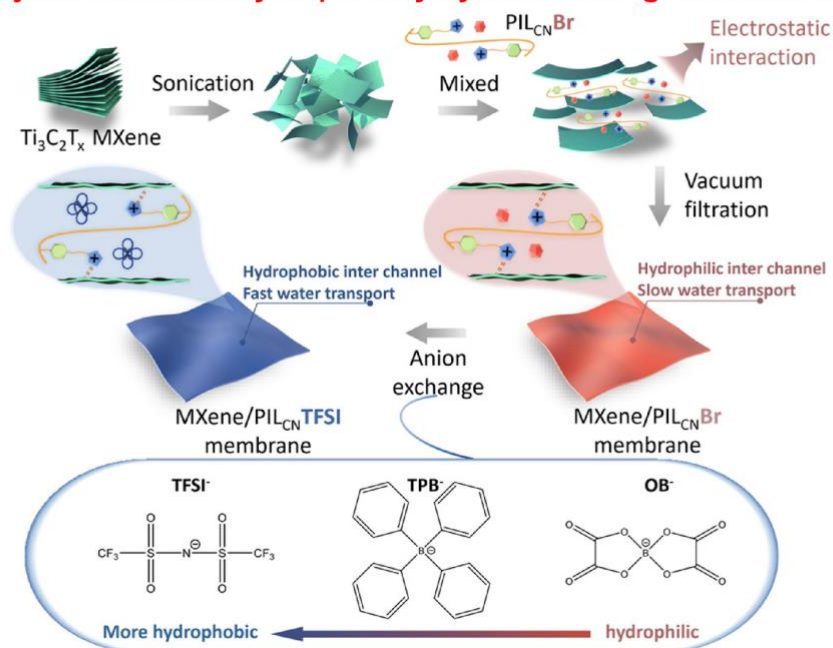
866



**(A) Accelerate water transport by grafting hydrophobic groups**



**(B) Adjust membrane hydrophilicity by intercalating external molecules**



868

869 **Figure 5.** The surface wettability control of 2D nanolaminate membranes based on the

870 chemical modification. (A) Averaged speed distribution of the first layer of water

871 molecules in the pristine (left) and methyl functionalized (right) MoS<sub>2</sub> nanochannel and

872 its projection along the channel direction ( $V_x$ ). **(B)** Schematic illustrating the  
873 preparation of MXene/PIL membranes with tailorable hydrophilicity. Images adapted,  
874 with permission, from [46,62,93,96].

875

876

877

878 **Highlights**

879 Membranes are key for many important technological domains including energy  
880 storage, energy conversion, water treatment and separation of chemicals.

881 Exfoliated two-dimensional (2D) materials, when used as membrane building blocks,  
882 lead to remarkable separation capabilities for gas separation, micropollutant removal,  
883 desalination and organic solvents.

884 The sieving behavior of nanolaminate membranes is controlled by the properties of the  
885 nanochannels formed between the nanosheets, which result from the subtle balance  
886 between attractive van der Waals forces and repulsive forces resulting from hydration  
887 and electrostatic repulsion.

888 Strategies have been proposed to tailor the surface characteristics and physiochemical  
889 properties of the 2D nanosheets, thereby enabling the creation of tailored transport  
890 pathways with intriguing nanofluidic behavior.

891

892

893 **Glossary**

894 **2D materials:** A family of materials characterized by an atomic thickness, exhibiting a  
895 sheet-like morphology. By extension, the definition of 2D materials has broadened to  
896 encompass materials with negligible thickness in comparison to their lateral dimensions  
897 (height and width).

898 **Nanochannel:** The confined space within the nanometer range between the nanosheets  
899 in the nanolaminates.

900

901

902

903

904 **Interlayer space:** The interatomic distance between two successive nanosheets in the  
905 nanolaminate. The value is obtained from the position of the (002) peak in the X-ray  
906 diffraction pattern or high resolution electron microscopy

907 **Capillary width:** The space accessible in the nanochannel. The capillary width is  
908 calculated by subtracting the thickness of the nanosheets to the interlayer space

909 **Membranes:** A semi-permeable material employed to separate two regions and  
910 facilitate the selective diffusion of chemical species.

911 **Functionalization:**

912 The process of surface modification of (nano)materials with molecules or functional  
913 groups involves functionalization, which can be either covalent or non-covalent.  
914 Covalent functionalization induces the formation of a chemical bond, while non-  
915 covalent methods rely on physical forces such as van der Waals or electrostatic  
916 interactions.

917 **Rejection:** The separation capability of a membrane refers to its ability to isolate a  
918 specific chemical species from others. This property is commonly quantified as a  
919 percentage, with 100% rejection indicating complete prevention of the substance from  
920 crossing the membrane.

921 **Permeance:** A quantitative metric assessing the flow through a porous material.

922 **Slip length:** A parameter used to characterize the interaction of a fluid with a solid  
923 surface. A high slip length indicates minimal interactions between fluid molecules and  
924 the solid surface.